A multiscale model to design therapeutic strategies that overcome drug resistance to tyrosine kinase inhibitors in multiple myeloma

Anass Bouchnita, Vitaly Volpert, Mark Koury, Andreas Hellander

A multiscale model to design therapeutic strategies that overcome drug resistance to tyrosine kinase inhibitors in multiple myeloma

Anass Bouchnita[a,b,*], Vitaly Volpert[c,d,e], Mark J. Koury[f], Andreas Hellander[a]

[a] *Division of Scientific Computing, Department of Information Technology, Uppsala University, Uppsala 75105, Sweden*
[b] *Ecole Centrale Casablanca, Ville Verte, Bouskoura, 20000 Casablanca, Morocco*
[c] *Institut Camille Jordan, Université Lyon 1, Villeurbanne 69622, France*
[d] *INRIA Team Dracula, INRIA Lyon La Doua, Villeurbanne 69603, France*
[e] *Peoples Friendship University of Russia (RUDN University), 6 Miklukho-Maklaya St, Moscow 117198, Russian Federation*
[f] *Vanderbilt University Medical Center, Nashville, TN 37232-6307, USA*

Drug resistance (DR) is a phenomenon characterized by the tolerance of a disease to pharmaceutical treatment. In cancer patients, DR is one of the main challenges that limit the therapeutic potential of the existing treat-ments. Therefore, overcoming DR by restoring the sensitivity of cancer cells would be greatly beneficial. In this context, mathematical modeling can be used to provide novel therapeutic strategies that maximize the efficiency of anti-cancer agents and potentially overcome DR. In this paper, we present a new multiscale model devoted to the interaction of potential treatments with multiple myeloma (MM) development. In this model, MM cells are represented as individual objects that move, divide, and die by apoptosis. The fate of each cell depends on intracellular and extracellular regulation, as well as the administered treatment. The model is used to explore the combined effects of a tyrosine-kinase inhibitor (TKI) with a pentose phosphate pathway (PPP) inhibitor. We use numerical simulations to tailor effective and safe treatment regimens that may eradicate the MM tumors. The model suggests that an interval for the daily dose of the PPP inhibitor can maximize the responsiveness of MM cells to the treatment with TKIs. Then, it demonstrates that the combination of high-dose pulsatile TKI treatment with high-dose daily PPP inhibitor therapy can potentially eradicate the tumor.The predictions of numerical simulations using such a model can be considered as testable hypotheses in future pre-clinical experiments and clinical studies.

1. Introduction

Drug resistance (DR) is a well-known phenomenon that circumvents the sensitivity of cancer cells to treatments. DR can be acquired by different mechanisms and frequently can be induced by chemotherapy itself. In fact, chemotherapy can eliminate susceptible clones, thereby altering the composition of cancers and making them more aggressive due to the survival of resistant clones. Chemotherapy can also alter the metabolism or the genetics of the cancerous cells and, thereby, increase their resistance to the treatment [1]. In this context, mathematical modeling can be used to gain insights on the mechanisms that confer DR to cancer cells, as well as to design novel therapeutic strategies that can overcome this resistance and restore the sensitivity of the tumor to the treatment.

To illustrate the applications of mathematical modeling in an effort to overcome drug resistance in cancer, we consider the case of multiple myeloma (MM). MM is a progressive hematological malignancy of plasma cells characterized by a complex genetic background. In MM, the epidermal growth factor receptor (EGFR) pathway is one of the commonly altered pathways with surface membrane EGFRs and their downstream signaling components Ras and Raf among the most commonly mutated proteins [2]. Some of the acquired mutations increase the expression of the corresponding protein such as EGFR, whereas others downregulate the inactivation of signaling proteins such as Ras and Raf. As a result, the concentration of active ERK, the EGFR tyrosine kinase-signaling pathway component that translocates to the nucleus, induces to an elevation of active transcription factors in the nucleus and promotes MM cell proliferation [3].

EGFR inhibitors represent attractive therapeutic agents for MM because they reduce the activation of EGFRs. Tyrosine Kinase Inhibitors (TKIs) such as erlotinib and gefitinib are a class of EGFR inhibitors that bind and inhibit EGFRs, thereby decreasing their specific kinase

* Corresponding author.
E-mail address: anass.bouchnita@centrale-casablanca.ma (A. Bouchnita).

activity, which leads to tyrosine phosphorylation in the Raf-Ras-MEK-ERK signaling pathway. These TKIs inhibit EGFR signaling and reduce the number and diameter of EGFR clusters that bind EGF on the cell surface [4]. Sorenafinib, another TKI that acts on the Raf-Ras-MEK-ERK signaling pathway, has activity against MM cells in vitro [5] but did not have anti-myeloma activity as a single agent in clinical trials. *In vitro*, the sensitivity of MM cells to these EGFR inhibitors is reduced by an accompanying resistance provoked by changes in the metabolism of the tumor cells [6]. These metabolic changes involve a shift in glucose metabolism to the pentose phosphate pathway (PPP) which promotes the proliferation of the cells [7]. The PPP pathway contributes to DNA synthesis in two major ways: 1) PPP supplies the pentose moiety of ribonucleotides and deoxynucleotides, and 2) chemical reduction of the cofactor nicotinamide adenine dinucleotide phosphate (converting NADP+ to NADPH) by the PPP is required for the activity of ribonucleotide reductase, the enzyme responsible for the conversion of ribonucleotieds to deoxynucleotides. As a result, high levels of DNA synthesis and MM cell proliferation can occur despite the inhibitory effects of the TKIs.

Among limited methods that can be used in order to overcome the resistance to EGFR inhibitors in MM cells, inhibition of the PPP with the antimetabolite 6-aminonicotinamide (6-AN) reduced the resistance of MM in vitro [7]. The proliferation rate of MM cells without *N-Ras* and *K-Ras* mutations was reduced to 25% of control when 6-AN was administered. Resistance was restored when NADPH was added [7] which indicates that the EGFR inhibitors upregulate the expression of this metabolic cofactor. However, the clinical use of 6-AN represents a challenge due to its high toxicity [8] and rapid clearance [9]. Therefore, it is difficult to develop effective and safe treatment regimens that combine both an EGFR inhibitor and a PPP inhibitor. However, this challenging problem can be approached and appropriately examined using mathematical modeling. With the results of mathematical modeling, the most appropriate schedules and doses of the two interacting treatments, TKI and 6-AN, can be tested in subsequent pre-clinical and clinical in vivo studies.

Mathematical modeling has been used previously to gain insights into the mechanisms that confer DR to cancer cells and predict the outcome and anti-cancer therapies. The first type of model that was developed uses ordinary differential equations (ODEs) to describe the intraclonal heterogeneity of tumors and how it evolves during chemotherapy [10,11]. The advantage of this type of model is the potential to study intraclonal heterogeneity and its evolution theoretically and numerically [12]. In addition, ODE-based models can be used to study the changes that take place at the intracellular level during the treatment [13]. In this context, global sensitivity analysis can be used to determine the intracellular proteins that most affect the responsiveness of tumor cells to the treatment. Furthermore, ODEs can be used to simulate the pharmacokinetics and pharmacodynamics (PK-PD) of treatments and the accompanying emergence of drug resistance [14]. The second type of model that studied drug resistance in cancer uses partial differential equations (PDEs) to represent the interaction between tumors and their micro-environment. Spatiotemporal dynamics of solid tumor growth during chemotherapy can be studied using this approach [15]. Other models that use PDEs consider the population of cells to be structured by a phenotypic variable [16]. An advantage of these models is the potential to use the optimal control theory in order to design optimal treatment strategies that can potentially overcome DR [17].

Agent-based modeling is another approach that can be used to simulate the effects of DR and chemotherapy on tumor growth. In this type of model, cells are represented as individual agents that can interact with their local environments. Agent-based modeling provides a high-fidelity description of cell-cell interactions. An *in silico* study in this category revealed that the optimal strategy used to overcome DR should correspond to the specific mechanism that induces the resistance [18]. Individual-based models can also be structured by cell phenotype. In this case, simplified PDE models could be derived that yielded the same results as the more sophisticated individual-based models and permitted them to be studied analytically [16]. Hybrid discrete-continuous models are another type of models that can be used to describe tumor growth during chemotherapy. These models use a discrete representation of cells and a continuous description of the extracellular and intracellular regulation networks, thereby combining mechanisms that take place at several scales in a single model. A hybrid discrete-continous model has shown that angiogenesis may contribute to the emergence of DR to TKIs [19]. Another model has revealed that the administration of EGF can overcome the resistance of lymph node metastases to immunotherapy with programmed death-1/programmed death-ligand1 blockade [20]. The role of cell-cycle mediated drug resistance and intraclonal heterogeneity was investigated using a hybrid multiscale model [21]. PK-PD modeling of anti-cancer drugs can be easily integrated within these models, which increases their practicality and usefulness [22]. We have previously studied intraclonal heterogeneity and response to the treatment using hybrid discrete-continuous models [23,24].

In this work, we develop a multiscale model to describe the development of MM tumors and their response to the targeted therapy with TKIs. In this new model, cells are represented as elastic spheres that move, divide, and undergo apoptosis. The fate of each cell is regulated by intracellular and extracellular networks as well as its response to the treatment. ODEs are used to describe intracellular signaling and metabolism while PDEs are used to simulate the concentration of cytokines and drugs in the extracellular matrix. We introduce treatment with gefitinib and 6-AN using an appropriate pharmacokinetic submodel, and we consider that the gefitinib induces DR in MM cells. We use numerical simulation to quantify the effects of metabolic shifts on the acquisition of drug resistance to TKIs by MM cells. Then, we evaluate the response of MM tumors to different treatment combinations of gefitnib and 6-AN.

2. A hybrid discete-continuous model of MM progression and its interaction with the treatment

We develop here a hybrid discrete-continuous model to describe the action of EGFR inhibitors on MM cells, and thereby, to understand the resistance to TKIs in MM and to develop therapeutic strategies that can potentially overcome it. We consider a 2D domain corresponding to a $200\,\mu m \times \mu m$ section of the bone marrow, the site of MM tumors. We simulate the response of MM tumors in this area to different treatment protocols as shown in Fig. 1.

2.1. Cell motion

The model consists of cells represented as elastic spheres. Each cell is characterized by the coordinates of its center x_i as well as its radius. In the process of cell division, cells increase their radius and push the adjacent cells, if the distance between their centers h_{ij} is less than the sum of their radii $r_1 + r_2$. To describe the elastic force between cells, let us consider two cells whose centers are denoted by x_i and x_j. The motion of each cell is described by Newton's second law:

$$m\ddot{x}_i + \mu\dot{x}_i - \sum_{j\neq i} f_{ij} = 0, \tag{1}$$

where m is the mass of the cell, μ is the friction factor due to contact with the surrounding medium. The repulsive force between two cells is given by the formula:

$$f_{ij} = \begin{cases} K\frac{h_0 - h_{ij}}{h_{ij} - (h_0 - h_1)} & , \quad h_0 - h_i < h_{ij} < h_0 \\ 0 & , \quad h_{ij} \geq h_0 \end{cases},$$

where h_{ij} is the distance between the centers of the two cells i and j, h_0 is the sum of their radii, K is a positive parameter. The force between the

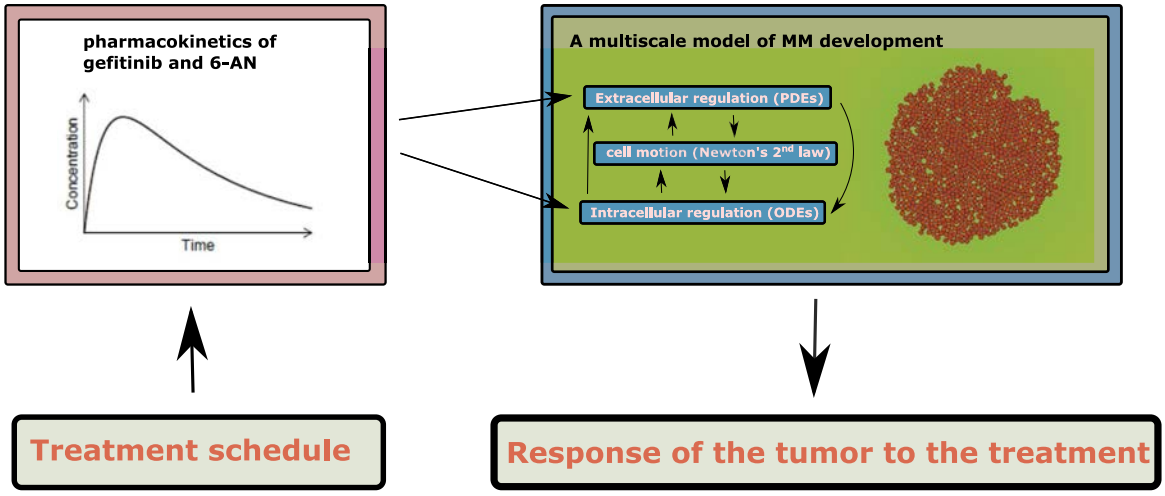

Fig. 1. A representation of the architecture of the model. Treatment schedules are introduced in order to simulate the pharmacokinetics of gefitinib and 6-AN. The two drugs affect the intracellular and extracellular regulation of MM cells. In this way, the response of the tumor to the treatment is predicted.

cells tends to infinity if h_{ij} decreases to $h_0 - h_1$. Cell elasticity was considered to properly describe the reorganization of the tissue following the division of a cell.

2.2. Intracellular regulation

The division of individual MM cells depends on the number of synthesized proteins, which depend upon the translation of mRNAs transcribed from specific genes, and the completion of nuclear DNA replication. The rate of this process depends on the number of active transcription factors in the nucleus as well as on the intracellular concentrations of ribonucleotides and deoxyribonucleotides required for the DNA synthesis. The activation of transcription factors depends on the translocation of active ERK [25], whereas the production of ribonucleotides and deoxyribonucleotides is regulated by the intracellular concentration of reduced nicotinamide adenine dinucleotide phosphate (NADPH), which is the product of the PPP activity [26]. We have represented these mechanisms in Fig. 2. We use the following system of equations to describe the intracellular regulation of each cell:

$$\frac{dE_i}{dt} = \frac{\alpha_1 G_F(\mathbf{x_i}, t)(E^0 - E_i)}{1 + \beta_1 I_e(\mathbf{x_i}, t)} - d_1 E_i, \tag{2}$$

$$\frac{dT_i}{dt} = \alpha_2 E_i (T^0 - T_i) - d_2 T_i, \tag{3}$$

$$\frac{dN_i}{dt} = \beta_3 (N^0 - N_i) + \alpha_3 I_e(\mathbf{x_i}, t)(N^0 - N_i) - \gamma_3 A_e(t) N_i - d_3 N_i, \tag{4}$$

$$\frac{dD_i}{dt} = \alpha_4 R_i N_i, \tag{5}$$

$$\frac{dA_i}{dt} = \alpha_5 A_e(t) - d_5 A_i, \tag{6}$$

Eq. 2 describes the concetration of active ERK in each cell. The first term in the right-hand side of this equation describes the cumulative effect of EGFR/ERK signaling. This signaling is upregulated by the concetration of ERK inside the cell and blocked by the external EGFR inhibitors. The second term corresponds to the inactivation of ERK.

Next, Eq. 3 represents the activation of transcription factors (TFs) in the nuleus (T_i), a process that depends on the translocation of ERK molecules. In parallel, we describe the production of the cofactor NADPH (N_i) using Eq. 4. NADPH is a product of the PPP that participates in the formation of the ribonucleotides and deoxyribonucleotides. In this equation, the first term in the right-hand side of this equation characterizes the reduction of NADP+ to NADPH by the PPP under normal conditions. The second term describes the increase in the production of NADPH caused by the resistance to the EGFR inhibitors (via the induction of the PPP). The third term in the right-hand side of the equation describes the decrease in NADPH caused by the PPP inhibitor 6-AN. The last term represents the oxidation of NADPH to NADP+.

Then, Eq. 5 simulates the production of DNA. In this equation, R_i describes the rate of DNA replication which depends on the number of transcription factors in the nucleus (T_i). Therefore, we consider that $R_i = \alpha_4^* T_i$.

The cell dies by apoptosis if the concentration of synthesized DNA in the cell does not achieve a threshold D^*. Otherwise, it divides and gives rise to two daughter cells.

Finally, we use Eq. 6 to describe the concentration of 6-AN inside each cell. The first term in the right-hand side of that equations describes the accumulation of intracellular 6-AN by the cell and the second term describes its degradation.

2.3. Extracellular regulation

The fate of MM cells depends upon the extracellular concentration of two molecules: epidermal growth factor (G_f) and EGFR inhibitor (I_e). We describe their respective spatial concentrations using the following system:

$$\frac{\partial G_F}{\partial t} = D_{G_F} \Delta G_F - W_{G_F} G_F - b_1 G_F, \tag{7}$$

$$\frac{\partial I_e}{\partial t} = D_{I_e} \Delta I_e - W_{I_e} I_e - b_2 I_e, \tag{8}$$

Eq. 7 describes the concentration of the epidermal growth factor (G_f). In this equation, D_{G_F} represents the diffusion coefficient, W_{G_F} is the consumption rate by tumor cells determined at the center of the of MM cells, and b_1 is the degradation/clearance rate of the cytokine. We prescribe Robin condition at the four boundaries of the domains to simulate the influx of EGF proteins to the computational domain. This imposed boundary condition is given as follows:

$$\frac{\partial G_F}{\partial n} = G_{F0}(G^0 - G_F),$$

where G_{F0} is a positive constant. Similarly, we describe the concentration of the EGFR inhibitor as follows:

Eq. 8 simulates the concentration of the EGFR inhibitor in the bone marrow section. In this equation, D_{I_e} is the diffusion coefficient, W_{I_e} is the consumption rate by tumor cells, and b_2 is the degradation/clearance rate of the inhibitor. This imposed boundary condition depends on

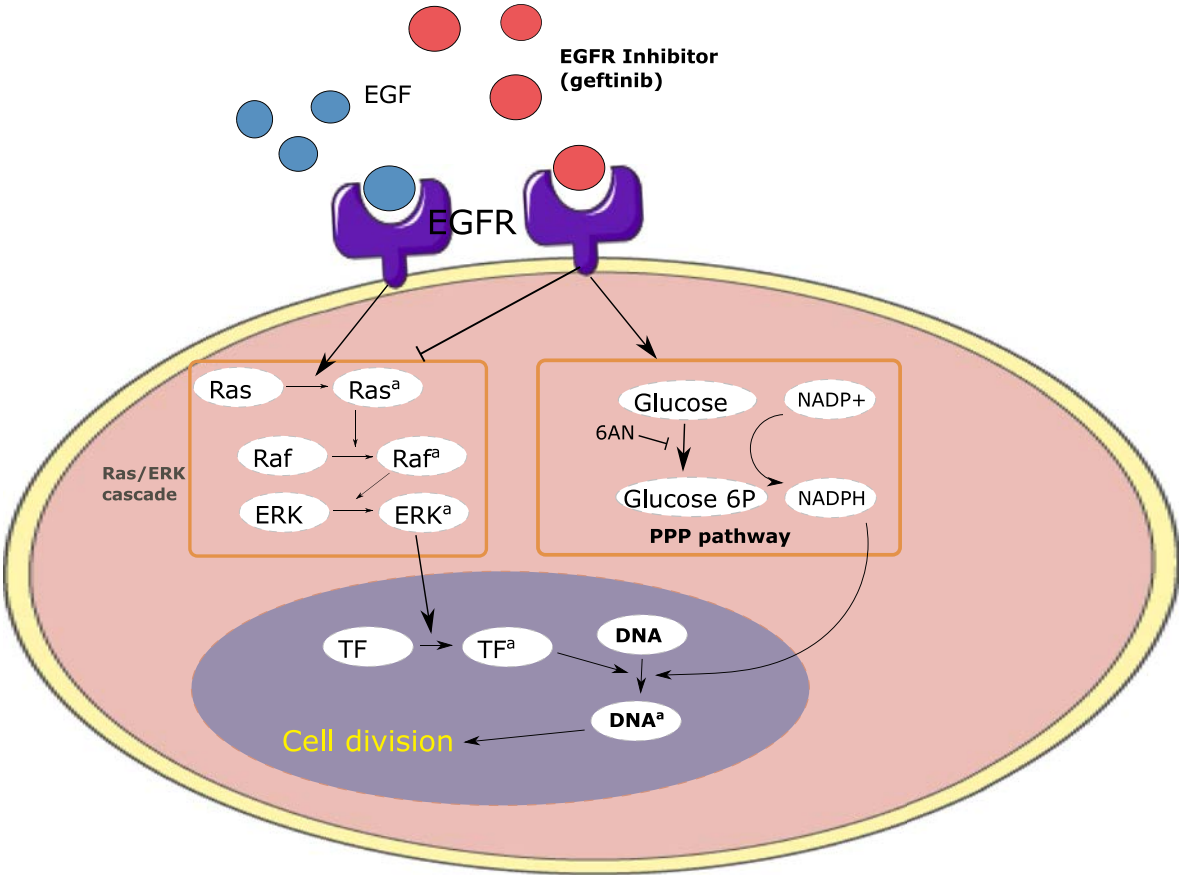

Fig. 2. Schematic representation of the action of gefitinib and erlotinib on MM cells and the acquired adaptive resistance. The two inhibitors (either gefitinib, as shown here, or erlotinib) block the EGFRs signaling and reduce EGFRs that can bind to their ligand, EGF. EGFR complexes activate the Ras protein and trigger the Ras/ERK cascade. The final output of this pathway, ERK, translocates to the nucleus and contributes to the activation of transcription factors (TFs). Active TFs control the rate of transcription of genetic information from DNA to RNA which participates in protein synthesis. Some of these proteins promote the growth and division of the cell. The inhibition of EGFR shifts glucose metabolism to the PPP when mutations in genes within the EGFR pathway are acquired. As a result, the production of the cofactor NADPH is upregulated. Increased ribonucleotides and deoxyribonucleotides secondary to increased NADPH leads to optimal nucleic acid synthesis allowing the growth and division of the cell despite the lower number of active transcription factors in the nucleus due to the EGFR inhibition. Cell membrane in yellow, cytoplasm in pink, and nucleus is violet. (For interpretation of the references to colour in this figure legend, the reader is referred to the web version of this article.)

the administration protocol ($I_e = I_0(t)$). The spatial concentration of 6-AN is not described due to its rapid clearance.

2.4. PK modeling of EGFR inhibitors and 6-AN

Gefinitib is a TKI which can be used in the targeted therapy of several types of cancer including MM. The regimen that is usually prescribed for this treatment consists of a daily dose of 250 mg. However, it is also possible to administer higher doses on fewer days such that the total administered dose at the end of the treatment remains the same. For example, a daily dose of 500 mg can be administered once every two days or a higher dose of 1000 mg can be prescribed once every four days. These treatment regimens were proven to be safe in clinical trials [27].

The agent 6-AN is administered to inhibit the PPP and, thereby, increase the sensitivity of MM cells to gefitinib therapy. 6-AN is potentially highly toxic and is capable of irreversible neurologic damage, which is related to cumulative administered dose [8]. The maximally tolerated dose is 5.6 mg/kg which can be, for example, administered at a dose of 0.2 mg/kg/d for a 4-week period or 0.4 mg/kg/d for a 2-week period. The highest dose that can be administered daily is 1.5 mg/kg. However, this dose can only be tolerated for 2–3 days due to neurotoxicity. Therefore, systemic modeling of the effect of 6-AN on the nervous system is not needed to conduct the present study. Under these circumstances, we evaluate the effects of treatment regimens consisting of both gefitinib and 6-AN on a MM tumor. In our simulations, we vary the treatment regimens of gefitinib and 6-AN each time. We assume that the treatment with 6-AN is terminated when the cumulative dose reaches 5.6 mg/kg to avoid toxicity. Gefitinib and 6-AN regimens are shown in Fig. 3.

We simulate the EGFR inhibitor-based treatment protocol using the ODE:

$$\frac{\partial I_0}{\partial t} = m_1 I(t) - n_1 I_0, \tag{9}$$

where $I(t)$ is a time-dependent function that describes the treatment protocol. It is equal to a constant value which corresponds to the administered dose I until the onset of action time is elapsed and to zero at other times. m_1 and n_1 are two positive constants. The onset of action for gefitinib is considered to be 4.5 h [28]. We use the same type of equation to describe the pharmacokinetics of 6-AN:

$$\frac{\partial A_e}{\partial t} = m_2 A(t) - n_2 A_e. \tag{10}$$

where $A(t)$ corresponds the dose A after the administration of 6-AN until the onset of action time exprires and to zero at other times. The 6-AN onset of action is estimated to be 30 min [9]. The last two equations

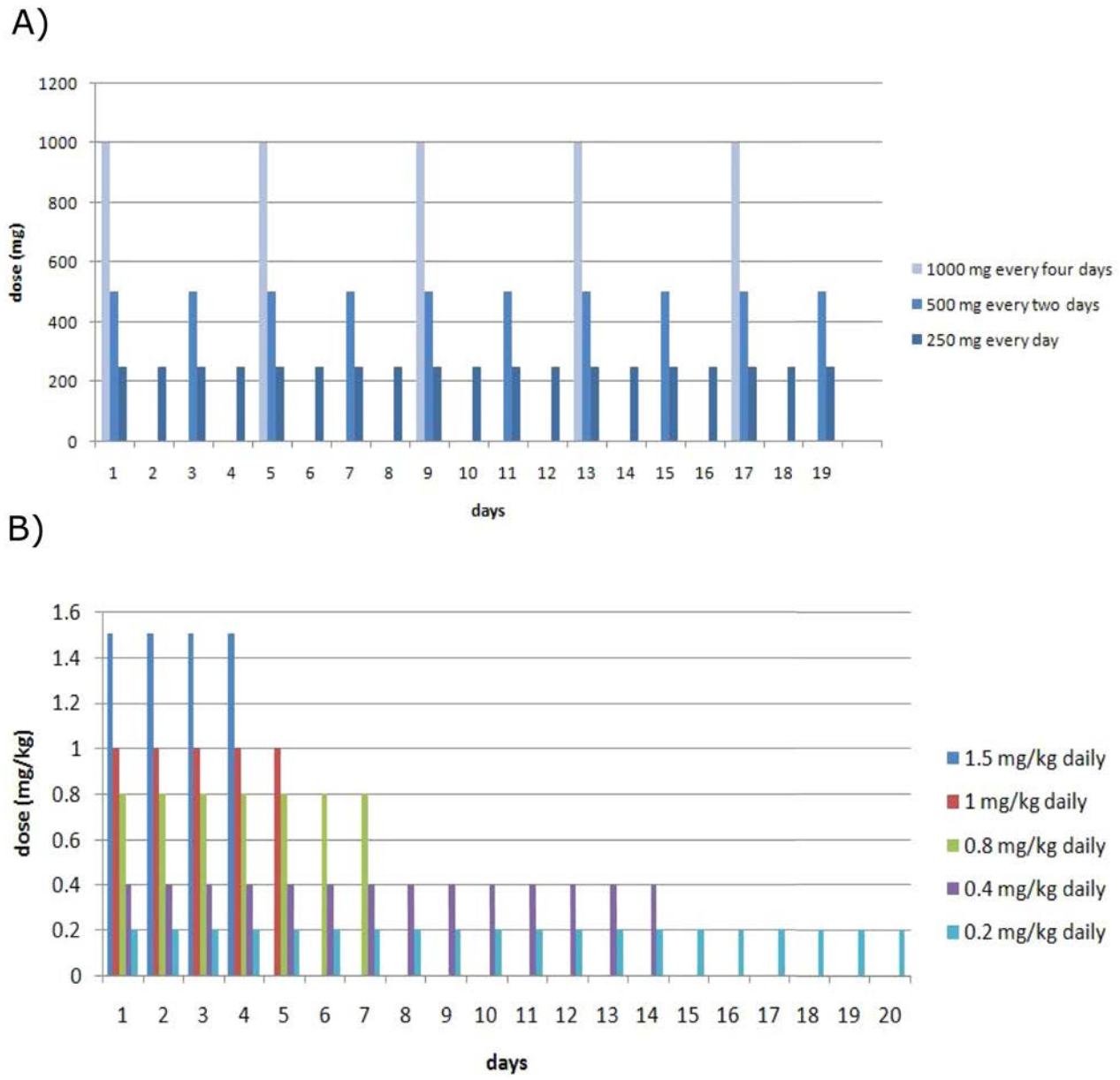

Fig. 3. Three regimens used for gefitinib (A) and five regimens used for 6-AN (B) therapies.

allow us to determine the respective tissue concentrations of EGFR and 6-AN as functions of the administered drug protocols. Drug metabolism is considered implicitly through the choice of the parameters.

2.5. Model implementation

We determined the values of some model parameters from the literature. These parameters include the diffusion coefficient of EGF as well as the pharmacokinetics properties for gefitinib and 6-AN. The parameters m_1 and m_2 were fitted by comparing with experimental measurement for the tissue concentrations of gefitinib [28] and 6-AN [9] when different doses are administered. Next, we have estimated the parameters that describe the intracellular regulation of MM cells by numerically solving the system (2)-(6) separately in the absence of treatment. A threshold of produced DNA (D^*) was determined such that the cell divides when it is sufficiently exposed to EGF. Then, the treatment was introduced and the parameters α_3 and γ_3 were fitted to reproduce experimental findings described in Fig. 4A of the study Chen et al. 2015 [7]. We provide the values of parameters in Table 1 of the Appendix.

The code was implemented in C++ in an object-oriented programming (OOP) architecture. The software ParaView was used to visualize the results. The CPU time for each simulation is around 50 min on a computer with four cores and 6 GB of RAM. Details of the numerical implementation of the hybrid model can be found in the appendix of a previous work [23].

3. Results

3.1. Parameter calibration and model validation

As previously mentioned, some of the parameters were taken from the literature while the rest were fitted to reproduce experimental findings in [7]. The experiments shown in Fig. 4A of this work quantify the proliferation of MM cells in normal conditions and under treatment with gefitinib and/or 6-AN. The proliferation of these cells is slightly

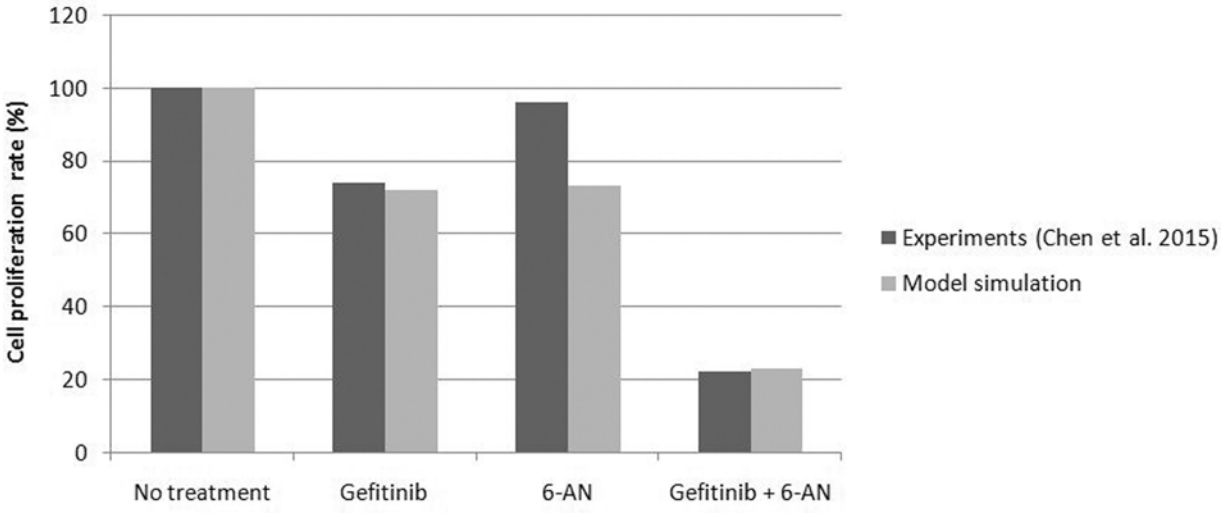

Fig. 4. Quantitative validation of the model showing the percent of proliferating rate of MM cells exposed 5 μM gefitinib and/or 0.4 mg/kg/day of 6-AN during 52 h. Model parameters were calibrated such that the simulated rate of cell proliferation approximate the observed ones in the experiments of Chen et al. 2015 [7].

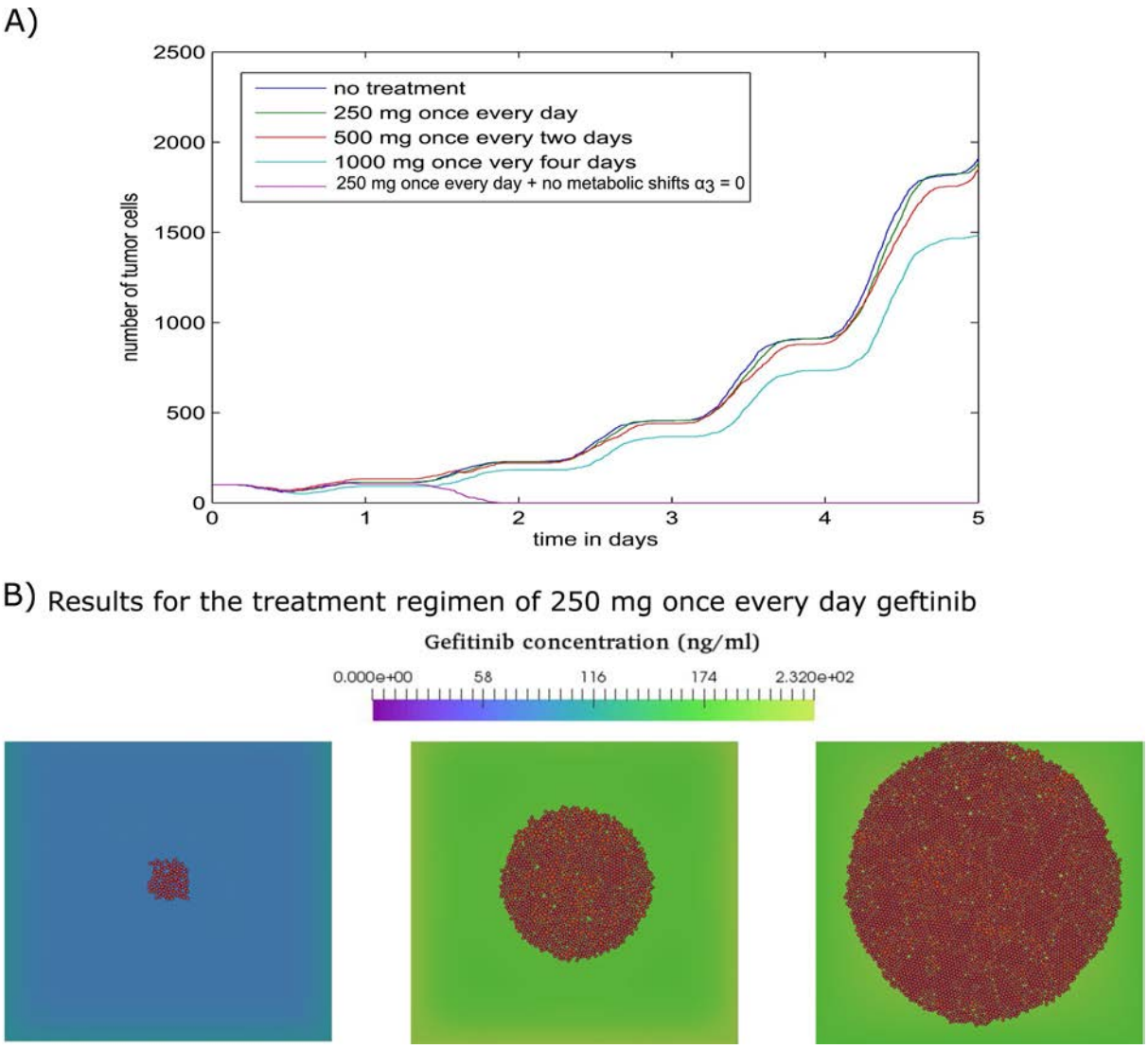

Fig. 5. A) The effect of gefitnib therapy and induced resistance on the number of cells in the tumor. Treatment with 6-AN is not considered in any of these simulations. B) Three stages of MM tumor resistance to gefitinib and growth in numerical simulations (from left to right).

decreased when a dose of 5 μM gefitinib is administered to the tumor during 48 h. It only decreases significantly when gefitinib and 6-AN, the PPP inhibitor, are both administered. The rate of cell proliferation, which is calculated as the percent of cells that divide at the end of their lifetime, was used as a metric to calibrate the model using the experimental data. We began by considering the case in which a gefitinib dose of 5 μM is administered in vitro during 48 h and computing the proliferation rate in this period of time. This corresponds to a tissue concentration of $I_e = 2.23 mg/ml^{-1}$ because the molecular mass of geftinib is equal to 446.902 g/M. In this case, we fit the parameter α_3 such as the proliferation rate is only reduced by approximately 25%.

Next, we introduce the effect of the PPP inhibitor 6-AN. In the absence of an indication of the 6-AN dose administered in the previous experiments, we consider a daily administration of 0.4 mg/kg once daily because it is the dose that was used in clinical settings [8]. We fit, γ_3, the rate of PPP inhibition by 6-AN, such that the simulated rate of cell proliferation corresponds to approximately 22%, similar to the experimental results [7]. Finally, we simulate the case where only 6-AN is administered by keeping the same parameter set as before and $I_e = 0\ mg/ml$. In this case, the simulated proliferation rate is slightly reduced than the experimentally observed one. However, it is not possible to improve the model prediction for this case, as changing any of the parameters would result in a change of the model predictions for the other cases. We show the experimentally observed vs. the numerically simulated rates of cell proliferation in Fig. 4 using 5 μM gefitinib and 0.4 mg/kg/day of 6-AN.

3.2. Numerical simulations confirm the role of metabolic shifts in confering DR to continuous and pulsatile gefitinib treatment

We begin by studying the dynamics of tumor growth during gefitinib treatment. We consider an initial MM tumor consisting of approximately 100 cells, with each cell at the beginning of its cell cycle. Numerical simulations predict that in the absence of the treatment, MM cells divide with a probability of approximately 100%, similar to the experimental data [7] (Fig. 5, A). To evaluate the response of MM cells to gefitinib, we repeat the tumor growth simulation under the same conditions, and we introduce gefitnib therapy. First, we consider the commonly prescribed treatment regimen of a 250 mg dose every day. The treatment with this daily gefitinib dose does not decrease the proliferation rate of MM cells. Therefore, the tumor continues to grow and occupies the whole computational domain (Fig. 5, A and B). Thus, administration of gefitinib alone is not sufficient to eliminate the tumor due to drug resistance resulting from metabolic shifts that upregulate the PPP. In the absence of these metabolic changes affecting the PPP ($\alpha_3 = 0$), the model predicts that the tumor will be eliminated within few days by gefitinib (see curve of 250 mg + no metabolic shifts in Fig. 5, A).

We compare the effects of daily 250 mg dosing versus pulsatile, less frequent, but larger doses of gefitinib on the development of a MM tumor. We consider three schedules of gefitinib: 250 mg once every day, 500 mg once every two days, and 1000 mg once every four days. Numerical simulations predict that the three regimens cannot eliminate the tumor, as shown in Fig. 5, A. However, pulsatile treatments with

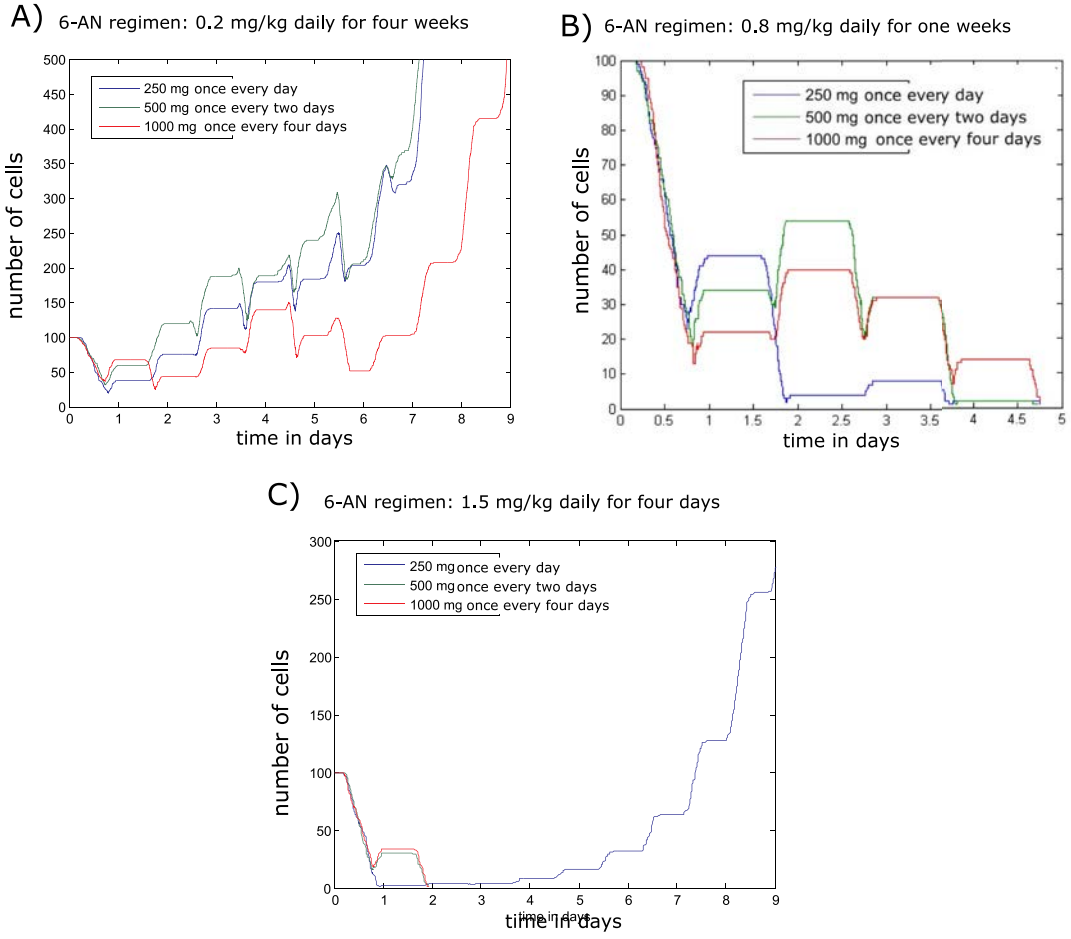

Fig. 6. The changes in MM cells population when treated with gefitinib and differing regimens of 6-AN. Each curve corresponds to one of the gefitinib regimens shown in the legend of the corresponding plot. The regimens of 6-AN are different in each case: A) 0.2 mg/kg daily for four weeks, B) 0.8 mg/kg daily for one week, C) 1.5 mg/kg daily for four days.

larger doses slightly reduce the growth rate of the tumor. The administration of 1000 mg once every four days results in more elimination of MM cells than the administration of 500 mg once every two days (Fig. 5, A).

3.3. The model suggests an interval of 6-AN dosing that maximizes the anti-MM effects of gefitinib

After studying the response of MM to gefitnib alone, we now introduce 6-AN to mitigate for the metabolic changes induced by gefitinib. 6-AN inhibits the PPP, thereby reducing the production of NADPH. As a result, the synthesis of DNA is restricted, and this restriction promotes apoptosis of the cell. To investigate the effects of 6-AN daily doses on the response of the tumor to gefitnib, we conduct numerical simulations for the various 6-AN-tolerated treatment schedules. When the administered 6-AN daily dose is low ($A \leq 0.3\, mg/kg$ each day), the PPP is not sufficiently inhibited to compensate for the metabolic shifts provoked by gefitinib. However, the proliferation rate of cells is reduced as the daily dose of 6-AN increases and begins to increase the rate of apoptosis. Therefore, the tumor grows steadily but more slowly with 6-AN than without it. The changes in MM cell populations during treatment with gefitinib in addition to a daily dose of 6-AN equal to 0.2 *mg/kg* is represented in Fig. 6, A.

When the daily dose of 6-AN is between 0.4 mg/kg and 0.9 mg/kg, the tumor is eliminated as shown in Fig. 7. The tumor is eradicated faster as the dose of 6-AN increases. Overall, the elimination of the tumor takes around three to six days depending on the administered 6-AN dose and the gefitinib treatment schedule (Fig. 6, B). In this case, the apoptosis of MM cells is mediated by the accumulated intracellular concentration of 6-AN and the availability of EGF.

When the administered daily dose of 6-AN exceeds 1 mg/kg, some MM cells survive after the termination of 6-AN therapy due to the short period of treatment with high daily doses and the rapid clearance of 6-AN. These surviving cells will form new foci of tumor cells which result in the relapse of MM (daily 250 mg gefitinib and 1.5 mg/kg 6-AN doses in Fig. 6, C and Fig. 8). Therefore, an interval exists for the daily dose for 6-AN which maximizes the elimination of MM cells.

3.4. Combination of high-dose pulsatile gefitinib treatment and high-dose 6-AN therapy promotes the rapid elimination of MM cells

The effects of gefitinib and 6-AN remain approximately the same when we consider pulsatile regimens for gefitinib. The two treatments eliminate the tumor when the daily prescribed dose of 6-AN is between 0.3 mg/kg and 0.9 mg/kg (Fig. 6, B and Fig. 9, A). However, when we combine a high 6-AN dose (higher or equal to 1.2 kg/mg daily) with

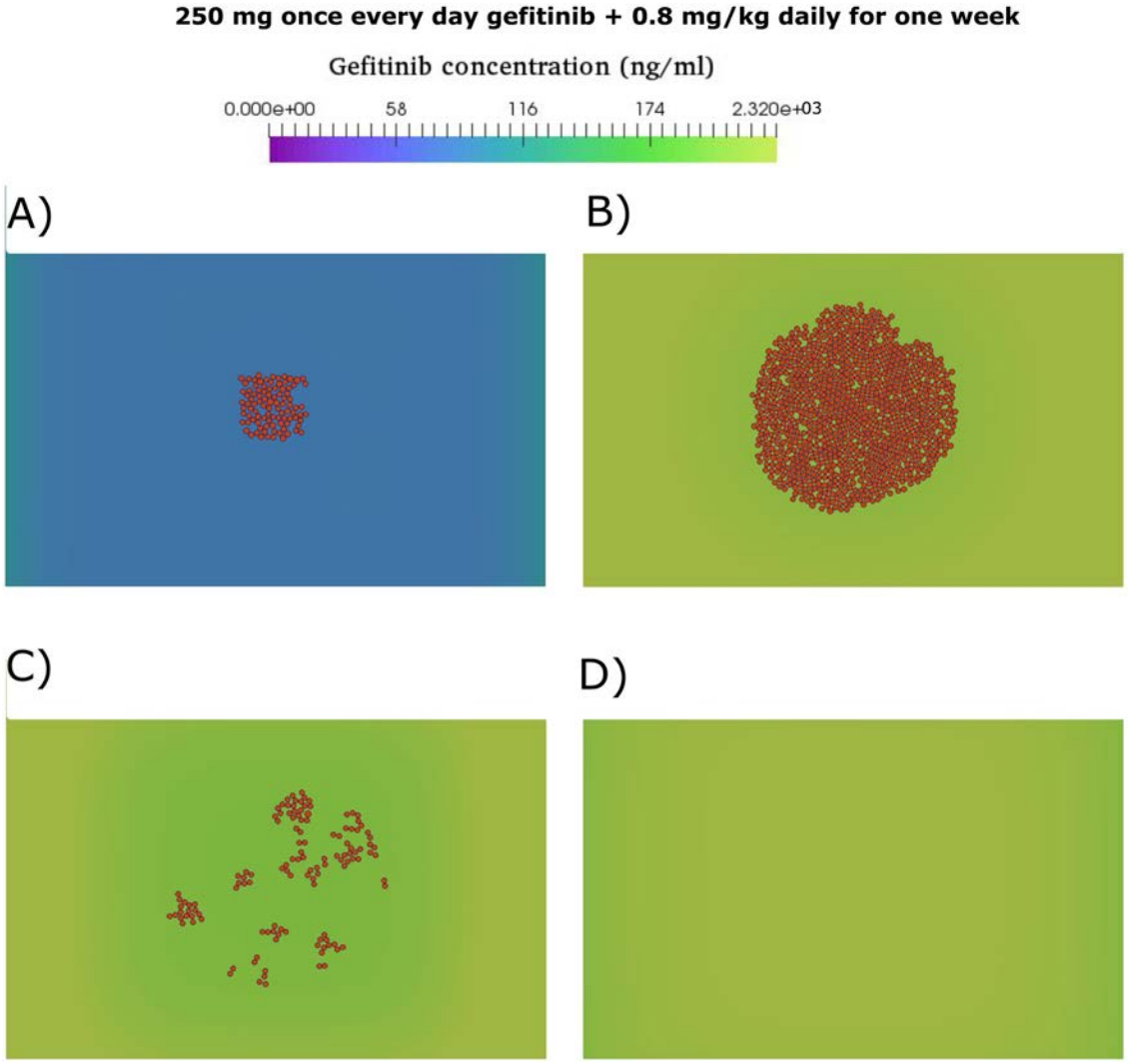

Fig. 7. Snapshots of a numerical simulation describing tumor elimination. A) The initial tumor consists of approximately 60 cells. B) The maximal expansion of the tumor. C) The elimination of the majority of tumor cells days after its expansion with only few niches of cells remaining. D) The complete eradication of the tumor.

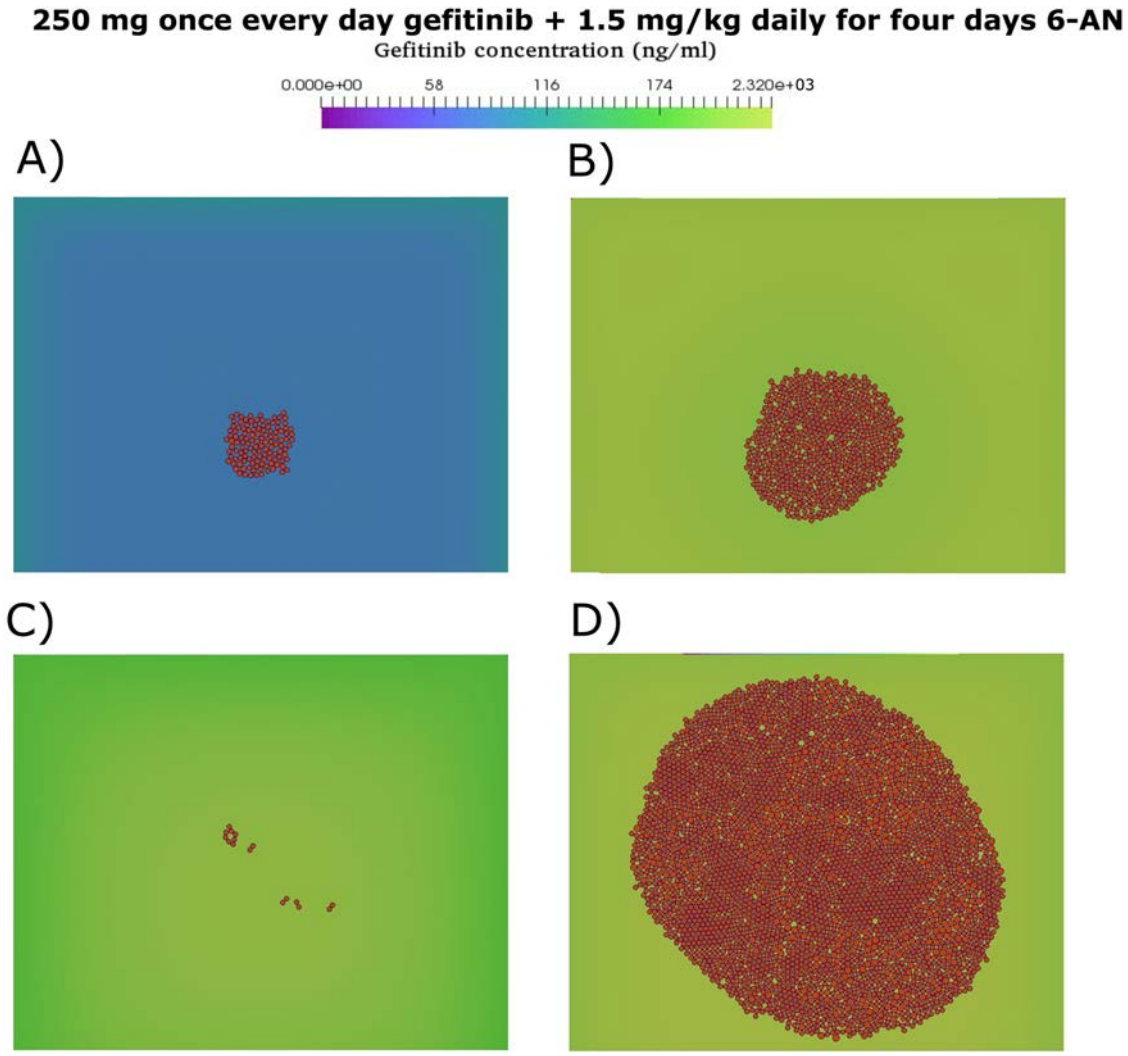

Fig. 8. Snapshots of a numerical simulation describing tumor relapse. A) The initial tumor. B) The maximal expansion of the tumor. C) The elimination of the majority of MM cells due to the combined EGFR and PPP inhibition except few cells. D) The surviving cells form new tumors which leads to tumor recurrence.

high-dose pulsatile gefitinib (1000 mg once every four days), then the tumor is eliminated within two days (Fig. 6, C). The elimination of the tumor is also observed when the maximally tolerated dose of 6-AN (1.5 kg/mg/d) is combined with a pulsatile gefitinib treatment consisting of 500 mg once every two days. We have summarized the MM tumor responses to the combination of various gefitinib and 6-AN treatment regimens in Fig. 9, A.

3.5. The level of PPP induction by gefitinib narrows down the interval of 6-AN that maximizes the elimination of MM cells

After understanding the global behavior of the model, we quantify the effects of the metabolic shifts induced by gefitinib on the response to the treatment with gefitnib and 6-AN combination. To achieve this, we administer a continuous treatment schedule of gefitnib and we vary the rate of PPP induction by gefitinib (α_3) as this is a parameter that is difficult to estimate from experimental data. We search for the interval of 6-daily AN dosing that eliminates the MM tumor for each value of α_3. As before, the treatment is terminated when the maximal administered dose of 6-AN reaches 5.6 mg/kg. The model shows that an increase in the rate of PPP upregulation by gefitinib would shrink the interval of 6-AN daily dosing that induces MM elimination (Fig. 9, B).

4. Discussion

This paper presents a modeling study of the response of MM tumors to targeted therapy with TKIs. The objective of this study is not to determine the dosing intervals that eliminate MM cells. In fact, such dosing intervals could depend on several things like the patient characteristics and the MM cells phenotype. Thus, the aim of this work is to generate testable treatment strategies for MM that combine a TKI with a PPP inhibitor. To achieve this, we have developed a multiscale model that describes the action of gefitinib and 6-AN on MM cells. First, we simulated the concentrations of gefitinib and 6-AN in the extracellular matrix using an appropriate pharmacokinetics model. These concentrations affect the extracellular and intracellular regulation of MM cells in the course of treatment. We began by studying the effects of gefitinib alone and predicted the outcome of continuous and pulsatile gefitinib therapy on MM. The model confirms that the metabolic changes provoked by gefitinib make MM cells resistant to this treatment as observed in the experiments [7]. Furthermore, the model reveals that the pulsatile administration of gefitinib is slightly more efficient than continuous dosing. This is in a good qualitative agreement with experiments in an animal study [29]. Numerical simulations were used to gain insights into the complex interaction between MM drug resistance and TKIs. We have shown that a 6-AN dosing interval exists which

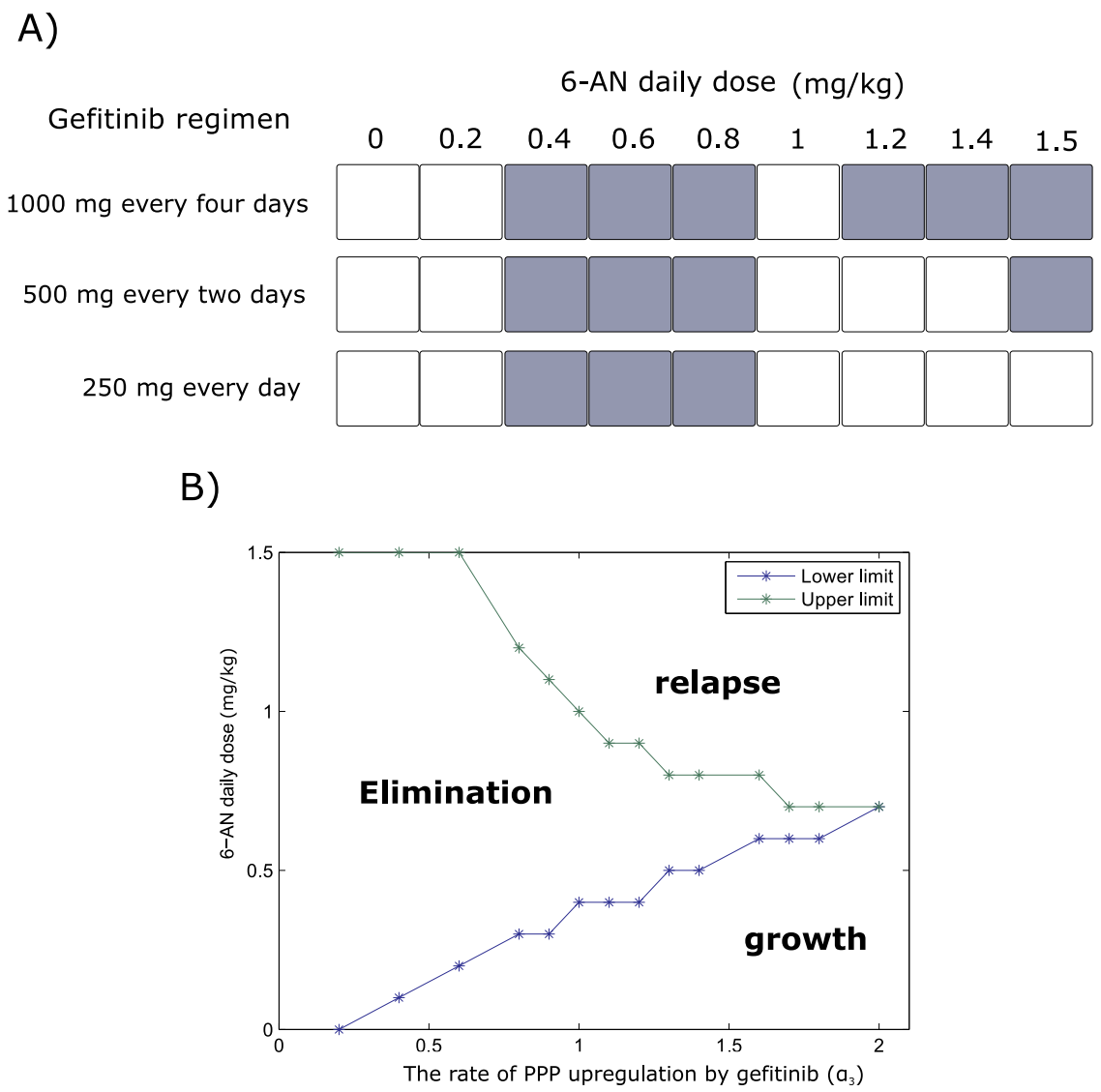

Fig. 9. A) Summary of the effects for the combination of gefitinib and 6-AN treatment regimens on MM tumors. The cases in blue correspond to the strategies resulting in the elimination of the tumor while the cases in white represent the strategies that result in the growth or the relapse of the MM tumor. B) The outcome of numerical simulations for different values for the rate of PPP upregulation by gefitinib (α_3, x-axis) and for different regimens of 6-AN (y-axis). The results show that the interval of 6-AN daily dose that maximizes the elimination of MM cells by gefitinib as a function of the upregulation rate of PPP by gefitinib. (For interpretation of the references to colour in this figure legend, the reader is referred to the web version of this article.)

maximizes the responsiveness of MM cells to the targeted therapy with TKIs. Moreover, our numerical simulations predict that the high-dose pulsatile gefitinib, combined with high-dose 6-AN, achieve maximal anti-myeloma effects.

The spatial effects play an important role in shaping the dynamics of the model. MM cells consume both EGF and gefitinib. Therefore, the relative location of each cell in the tumor determines its fate. For example, MM cells that are located in core of the tumor are not exposed to as high concentrations of gefitinib as MM cells located more peripherally in the tumor focus. As a result, these MM cells in the centrale core survive longer than the MM cells that are located at the periphery of the tumor, despite the relative scarcity of the available growth factors in this central area. It is these cells that will cause a relapse of the tumor after the termination of the treatment with 6-AN due to its toxicity. The multiscale nature of the model allowed us to describe the complex interactions that exist between MM cells and the treatment across several scales of biological organization. At the intracellular level, gefitinib and 6-AN cause metabolic changes to MM cells. Whereas the rate of gefitinib consumption by MM cells is determined by its concentration at the extracellular level. In addition, gefitinib reaches the tissue after being absorbed orally. Therefore, the model can be used to integrate experimental data obtained from a wide range of acquisition techniques such as flow cytometry and nano-imaging.

Some of the model parameters were obtained from the previous publications. These parameters include the onset of action and the half-life times of gefitinib and 6-AN. The diffusion coefficients and degradation rates of the extracellular cytokines were taken from previous publications. The rest of the model parameters were fitted in order to reproduce experimental results [7]. To ensure the robustness of the model, the cell cycle of all MM cells is set to the beginning of the G1 phase at the start of each simulation. Therefore, the model predictions remain the same for repeated simulations. As a result, the only remaining source of stochasticity in the model is a perturbation that is added to the cell cycle of each individual cell. While these small perturbations can slightly change the qualitative results, they are not sufficient to completely modify the dynamics of tumor growth. Assuming the cell cycles of MM cells to be synchronized also allowed us to interpret the obtained results and to conduct a systemic exploration of the

model. The goal of this model exploration study is to design optimal treatment strategies that combine an EGFR inhibitor with a PPP inhibitor. A sensitivity analysis study of the model parameters will be conducted in a forthcoming work. Furthermore, it is possible to implement algorithms that optimize the treatment regimens by solving an optimal control problem [30,31].

However, this study has some limitations that should be considered before testing the obtained treatment strategies in pre-clinical experiments and clinical studies. Some of these limitations are due to the limited availability of data in the literature. In particular, dose-effect curves of the combined effects of gefitinib and 6-AN could be used to calibrate the model, thereby making its predictions more reliable. In addition, the parameters that were taken from the literature correspond to experiments that were conducted on different organisms. For example, the parameters α_3 and γ_3 were fitted to reproduce in vitro experiments on human MM cells. While the pharmacokinetics parameters were taken from in vivo studies in rat and dog. As a result of these limitations, further calibration of the model is needed before it can be used to design clinical trials. Still, it demonstrates how the exploration of mathematical models could be used to develop treatment strategies that are based on drugs that are highly toxic and/or have a rapid clearance. Furthermore, the effectiveness of this drug combination is restricted to the MM tumors which do not harbor any mutations in the Ras and Raf oncogenes. These mutations cause a drug resistance of the treatment but with a different mechanism that involves the intracellular components of the EGFR internal signaling mechanism. We have studied the effects of alteration in the EGFR pathway using a 3D stochastic multiscale model in a previous work [32]. This model can be used in the future to investigate the impact of stochastic alterations in the intracellular regulation of cells on the response of MM tumors to chemotherapy. Finally, the potential resistance caused by MM intraclonal heterogeneity to these treatment protocols are not studied in the current model and will be investigated in a forthcoming work.

Declaration of Competing Interest

The authors declare that the research was conducted in the absence of any commercial or financial relationships that could be construed as a potential conflict of interest.

Acknowledgments

This work was supported by the Swedish research council (VR) under award no. 2015–03964 and by eSSENCE strategic collaboration of eScience. It was partially supported by the “RUDN University Program 5–100”, the Russian Science Foundation grant number 18-11-00171, and the French-Russian project PRC2307.

Appendix: model parameters

In this section we present the parameters that were considered in the numerical simulation. The list of parameters is provided in Table 1.

Table 1
Values of parameters used in simulations with the hybrid model. δ is an arbitrary length unit. NU refers to non-dimensional unit.

Parameter	Value	Unit	Description
dt	0.02	min	time step
D_{GF}	0.86	$\delta^2.\ min^{-1}$	diffusion coefficient of EGF [33]
D_{I_e}	1.5	$\delta^2.\ h^{-1}$	diffusion coefficient of gefitinib
W_{GF}	5×10^{-2}	min^{-1}	consumption rate of EGF by MM cells
W_{I_e}	5×10^{-2}	min^{-1}	consumption rate of gefitinib by MM cells
b_1	1×10^{-3}	min^{-1}	degradation rate of EGF
b_2	1×10^{-3}	min^{-1}	degradation rate of gefitinib
m_1	4.5×10^{-3}	$ml^{-1}min^{-1}$	rate of gefitinib distribution in the bone marrow [28]
n_1	2.77×10^{-3}	min^{-1}	degradation rate of gefitinib [28]
m_2	3.15×10^{-2}	$ml^{-1}min^{-1}$	rate of 6-AN distribution in the bone marrow [9]
n_2	2.15×10^{-2}	min^{-1}	degradation rate of 6-AN [9]
α_1	8×10^{-2}	$ml/ng^{-1}min^{-1}$	rate of ERK activation by EGF
d_1	1×10^{-3}	$min-1$	ERK degradation
β_1	5	ml/ng	rate of active ERK inhibition by geftinib
α_2	0.2	min^{-1}	transcription factors activation by ERK
d_2	0.1	min^{-1}	transcription factors degradation rate
β_3	0.1	min^{-1}	NADPH reduction rate
α_3	variable	$ml/ng.min$	rate of NADPH upregulation by gefitinib
γ_3	0.3	$ml/ng.min$	the rate of NADPH downregulation by 6-AN
d_3	0.1	min^{-1}	oxidation rate of NADPH to NADP+
α_4	0.2	min^{-1}	the rate of DNA synthesization
E^0	1	NU	maximal capacity of active and inactive EGFR in a cell
T^0	1	NU	maximal capacity of active and inactive TFs in a cell
N^0	1	NU	maximal capacity of active and inactive NADPH in a cell

References

[1] H. Zahreddine, K. Borden, Mechanisms and insights into drug resistance in cancer, Front. Pharmacol. 4 (2013) 28.

[2] M.A. Chapman, M.S. Lawrence, J.J. Keats, K. Cibulskis, C. Sougnez, A.C. Schinzel, C.L. Harview, J.-P. Brunet, G.J. Ahmann, M. Adli, et al., Initial genome sequencing and analysis of multiple myeloma, Nature 471 (7339) (2011) 467.

[3] C.C.-Y. Leow, S. Gerondakis, A. Spencer, MEK Inhibitors as a chemotherapeutic intervention in multiple myeloma, Blood Cancer J. 3 (3) (2013) e105.

[4] A. Abulrob, Z. Lu, E. Baumann, D. Vobornik, R. Taylor, D. Stanimirovic, L.J. Johnston, Nanoscale imaging of epidermal growth factor receptor clustering effects of inhibitors, J. Biolog. Chem. 285 (5) (2010) 3145–3156.

[5] M. Gentile, M. Martino, A.G. Recchia, E. Vigna, L. Morabito, F. Morabito, Sorafenib for the treatment of multiple myeloma, Expert Opin. Investig. Drug. 25 (6) (2016) 743–749.

[6] C. El Arfani, K. De Veirman, K. Maes, E. De Bruyne, E. Menu, Metabolic features of multiple myeloma, Int. J. Mol. Sci. 19 (4) (2018) 1200.

[7] Y. Chen, R. Huang, J. Ding, D. Ji, B. Song, L. Yuan, H. Chang, G. Chen, Multiple myeloma acquires resistance to EGFR inhibitor via induction of pentose phosphate pathway, Sci Rep. 5 (2015) 9925.

[8] F.P. Herter, S.G. Weissman, H.G. Thompson, G. Hyman, D.S. Martin, Clinical experience with 6-aminonicotinamide, Cancer Res. 21 (1) (1961) 31–37.

[9] D.L. Walker, J.M. Reid, P.A. Svingen, R. Rios, J.M. Covey, M.C. Alley, M.G. Hollingshead, I.I. Budihardjo, S. Eckdahl, S.A. Boerner, et al., Murine pharmacokinetics of 6-aminonicotinamide (nsc 21206), a novel biochemical modulating agent, Biochem. Pharmacol. 58 (6) (1999) 1057–1066.

[10] S. Michelson, J. Leith, Tumor heterogeneity: a review of the theory, DRUG NEWS AND PERSPECTIVES 6 (1993). 655–655

[11] J.C. Panetta, A mathematical model of drug resistance: heterogeneous tumors, Math. Biosci. 147 (1) (1998) 41–61.

[12] E. Gaffney, The application of mathematical modelling to aspects of adjuvant chemotherapy scheduling, J. Math. Biol. 48 (4) (2004) 375–422.

[13] G. Lebedeva, A. Sorokin, D. Faratian, P. Mullen, A. Goltsov, S.P. Langdon, D.J. Harrison, I. Goryanin, Model-based global sensitivity analysis as applied to identification of anti-cancer drug targets and biomarkers of drug resistance in the erbb2/3 network, Eur. J. Pharmaceut. Sci. 46 (4) (2012) 244–258.

[14] E. Hickey, Tools to define the relevance of PK/PD parameters to the efficacy, toxicity and emergence of resistance of antimicrobials. Curr. Opin. Drug Discov. Develop. 10 (1) (2007) 49–52.

[15] T.L. Jackson, H.M. Byrne, A mathematical model to study the effects of drug resistance and vasculature on the response of solid tumors to chemotherapy, Math. Biosci. 164 (1) (2000) 17–38.

[16] R.H. Chisholm, T. Lorenzi, A. Lorz, A.K. Larsen, L.N. De Almeida, A. Escargueil, J. Clairambault, Emergence of drug tolerance in cancer cell populations: an evolutionary outcome of selection, nongenetic instability, and stress-induced adaptation, Cancer Res. 75 (6) (2015) 930–939.

[17] C. Pouchol, J. Clairambault, A. Lorz, E. Trélat, Asymptotic analysis and optimal control of an integro-differential system modelling healthy and cancer cells exposed to chemotherapy, Journal de Mathématiques Pures et Appliquées 116 (2018) 268–308.

[18] S. Hamis, P. Nithiarasu, G.G. Powathil, What does not kill a tumour may make it stronger: in silico insights into chemotherapeutic drug resistance, J. Theor. Biol. 454 (2018) 253–267.

[19] X. Sun, L. Zhang, H. Tan, J. Bao, C. Strouthos, X. Zhou, Multi-scale agent-based brain cancer modeling and prediction of TKI treatment response: incorporating EGFR signaling pathway and angiogenesis, BMC Bioinform. 13 (1) (2012) 218.

[20] M.A. Benchaib, A. Bouchnita, V. Volpert, A. Makhoute, Mathematical modelling reveals that the administration of EGF can promote the elimination of lymph node metastases by PD-1/PD-L1 blockade, Front. Bioeng. Biotechnol. 7 (2019) 104.

[21] G.G. Powathil, M.A. Chaplain, M. Swat, Investigating the development of chemotherapeutic drug resistance in cancer: a multiscale computational study, arXiv:1407.0865(2014).

[22] Z. Wang, J.D. Butner, V. Cristini, T.S. Deisboeck, Integrated PK-PD and agent-based modeling in oncology, J. Pharmacokinet. Pharmacodyn. 42 (2) (2015) 179–189.

[23] A. Bouchnita, F.-E. Belmaati, R. Aboulaich, M. Koury, V. Volpert, A hybrid computation model to describe the progression of multiple myeloma and its intra-clonal heterogeneity, Computation 5 (1) (2017) 16.

[24] A. Bouchnita, N. Eymard, T.K. Moyo, M.J. Koury, V. Volpert, Bone marrow infiltration by multiple myeloma causes anemia by reversible disruption of erythropoiesis, Am. J. Hematol. 91 (4) (2016) 371–378.

[25] R.J. Orton, O.E. Sturm, V. Vyshemirsky, M. Calder, D.R. Gilbert, W. Kolch, Computational modelling of the receptor-tyrosine-kinase-activated MAPK pathway, Biochem. J. 392 (2) (2005) 249–261.

[26] K.C. Patra, N. Hay, The pentose phosphate pathway and cancer, Trend. Biochem. Sci. 39 (8) (2014) 347–354.

[27] Y. Zhu, Y. Du, H. Liu, T. Ma, Y. Shen, Y. Pan, Study of efficacy and safety of pulsatile administration of high-dose gefitinib or erlotinib for advanced non-small cell lung cancer patients with secondary drug resistance: a single center, single arm, phase ii clinical trial, Thoracic Cancer 7 (6) (2016) 663–669.

[28] D. McKillop, E. Partridge, M. Hutchison, S. Rhead, A. Parry, J. Bardsley, H. Woodman, H. Swaisland, Pharmacokinetics of gefitinib, an epidermal growth factor receptor tyrosine kinase inhibitor, in rat and dog, Xenobiotica 34 (10) (2004) 901–915.

[29] D.B. Solit, Y. She, J. Lobo, M.G. Kris, H.I. Scher, N. Rosen, F.M. Sirotnak, Pulsatile administration of the epidermal growth factor receptor inhibitor gefitinib is significantly more effective than continuous dosing for sensitizing tumors to paclitaxel, Clin. Cancer Res. 11 (5) (2005) 1983–1989.

[30] M. Oremland, R. Laubenbacher, Optimization of agent-based models: scaling methods and heuristic algorithms, J. Artif. Soc. Social Simul. 17 (2) (2014) 6.

[31] M.S. Oremland, Techniques for mathematical analysis and optimization of agent-based models. Virginia Tech, 2014 Ph.D. thesis.

[32] A. Bouchnita, S. Hellander, A. Hellander, A 3D multiscale model to explore the role of EGFR overexpression in tumourigenesis, Bull. Math. Biol. (2019) 1–22.

[33] R.G. Thorne, S. Hrabetová, C. Nicholson, Diffusion of epidermal growth factor in rat brain extracellular space measured by integrative optical imaging, J. Neurophysiol. 92 (6) (2004) 3471–3481.